Chemical Engineering Journal 308 (2017) 597–605

Contents lists available at ScienceDirect

Chemical Engineering Journal

journal homepage: www.elsevier.com/locate/cej

# Fabrication of β-cyclodextrin/poly (L-glutamic acid) supported magnetic graphene oxide and its adsorption behavior for 17β-estradiol

Luhua Jiang [a,b], Yunguo Liu [a,b,*], Shaobo Liu [c,*], Xinjiang Hu [d,e], Guangming Zeng [a,b], Xi Hu [e], Simian Liu [a,b], Shaoheng Liu [a,b], Binyan Huang [a,b], Meifang Li [a,b]

[a] College of Environmental Science and Engineering, Hunan University, Changsha 410082, PR China
[b] Key Laboratory of Environmental Biology and Pollution Control (Hunan University), Ministry of Education, Changsha 410082, PR China
[c] School of Metallurgy and Environment, Central South University, Changsha 410083, PR China
[d] College of Natural Resources and Environment, South China Agricultural University, Guangzhou 510642, PR China
[e] College of Environmental Science and Engineering Research, Central South University of Forestry and Technology, Changsha 410004, PR China

## HIGHLIGHTS

- Magnetic β-cyclodextrin/poly (L-glutamic acid) grafted onto GO is synthesized.
- CGMG can achieve rapid separation via using a magnet.
- CGMG shows decreased adsorption capacity at higher pH conditions.
- Sorption kinetic, isothermal and thermodynamic characteristics of E2 are explored.
- Regeneration of the magnetic adsorbent is conducted.

## ARTICLE INFO

*Article history:*
Received 28 June 2016
Received in revised form 12 September 2016
Accepted 13 September 2016
Available online 13 September 2016

*Keywords:*
17β-Estradiol
Adsorption
Poly-L-glutamic acid
β-Cyclodextrin
Graphene oxide

## ABSTRACT

A novel adsorbent, namely, β-cyclodextrin/poly (L-glutamic acid) supported magnetic graphene oxide (CGMG), was synthesized through a facile chemical route and its application as excellent adsorbent for 17β-estradiol (E2) removal from aqueous solution was also demonstrated. The characteristics of CGMG were investigated via using Fourier transform infrared spectrometer, X-ray photoelectron spectroscopy, Raman spectra, X-ray diffraction, vibrating sample magnetometer and Brunauer-Emmett-Teller surface area, respectively. Results indicated that CGMG was successfully prepared and the saturated magnetization could reach up to 0.09043 emu/mg. Meanwhile, investigation of adsorption behavior illustrated that the adsorption process could be better fitted by the pseudo-second-order and Langmuir models. Analysis of intraparticle diffusion model demonstrated that intraparticle diffusion was not the only rate-limiting step; however, both film diffusion and intraparticle diffusion were involved in the diffusion process. Thermodynamic study indicated that adsorption of E2 onto CGMG was spontaneous and endothermic. The E2 uptake by CGMG decreased in high pH values. However, it was insensitive to ionic strength variation (0.0–0.1 M). Moreover, the regeneration experiments illustrated that CGMG could be recovered, and it showed good recycling ability with ca. 88.7% of the initial sorption capacity after being used for sixth cycles.



## 1. Introduction

Recently, endocrine-disrupting chemicals (EDCs) pollution in the aquatic system has seriously aroused public concern. 17β-estradiol (E2) as one of the listed EDCs is widely detected in the aquatic environment as well as in drinking water [1,2]. It has been reported that the disrupting effect of E2 is 1000–10,000 times greater than that of nonylphenol [3]. However, it is difficult to effectively eliminate E2 from wastewater via conventional wastewater treatment processes such as activated sludge treatment and biofiltration [4]. Thence, it is desirable to seek significantly effective processes for the removal of E2 from aqueous solution. And up to now, several studies have explored the adsorptive removal of E2 via carbon-based materials such as granular

* Corresponding authors at: College of Environmental Science and Engineering, Hunan University, Changsha 410082, PR China (Y. Liu).
*E-mail addresses:* liuyunguo_hnu@163.com (Y. Liu), liushaobo23@aliyun.com (S. Liu).

http://dx.doi.org/10.1016/j.cej.2016.09.067
1385-8947/

activated carbon, chitin, chitosan, carbonaceous adsorbent prepared from industrial waste, and carbon nanotubes [4–8]. However, these adsorbents exhibited limited E2 adsorption capacity and/or suffered from poor extraction efficiencies. Moreover, almost all of them were found to be arduous in terms of recycle and reuse.

Poly-L-glutamic acid (PLGA), synthetized by using poly amino acid, possesses numerous functional groups and can be further chemically modified by inorganic and/or organic reagents [9]. PLGA has been successfully employed to fabricate scaffolds for drug delivery and tissue engineering applications and it is also used as biodegradable magnetic resonance imaging contrast reagent because of biocompatible polymeride [10–12]. Furthermore, PLGA has also been used as an effective adsorbent for the adsorption of several types of contaminants. For instance, Reyerson and Bhattacharyya utilized PLGA as adsorbent to remove ammonia gas and heavy metals from water, respectively [13,14]. Wang et al. investigated the adsorption of Cu(II) ions on $Fe_3O_4$/PLGA magnetic microspheres [15]. β-Cyclodextrin (β-CD), as a family of cyclic oligomers, is made up of glucopyranose units connected via α-1, 4 glycosidic bonds, and has a hydrophobic interior cavity and a hydrophilic exterior surface [16]. This characteristic enables it to selectively interact with a large variety of compounds, resulting in the formation of noncovalent inclusion complexes in their interior cavity [17]. Badruddoza et al. demonstrated the use of carbox ymethyl-β-cyclodextrin modified $Fe_3O_4$ nanoparticles as excellent nanoadsorbents for copper ions removal [18]. Consequently, the hybrid of β-CD/PLGA may be favorable for the effective removal of pollutants from water system due to the presence of abundant hydroxyl and amino functional groups. However, β-CD/PLGA hybrid exhibits a good water-dispersibility properties because of its hydrophilic surface, which make them rather difficult to realize solid-liquid separation via conditional separation methods (such as centrifugation and filtration) after adsorption [19,20].

Recently, many researchers have devoted extensive efforts to graft magnetic materials onto some adsorbents to improve their separation performances. For instance, Hu et al. [21] synthesized magnetic chitosan via loading $Fe_3O_4$ nanoparticles for adsorption of hexavalent chromium ions from aqueous solution. Fu et al. [22] reported the development of a novel hydrophilic-hydrophobic magnetic interpenetrating polymer networks (IPNs) for efficient removal of salicylic acid from aqueous solution. Kara et al. [23] reported that magnetic vinylphenyl boronic acid microparticles could act as an efficient adsorbent for Cr(VI) adsorption. However, grafting magnetic materials directly on adsorbents can reduce their adsorption capacity, since the magnetic nanoparticles are capable of occupying some adsorption sites on the surfaces of adsorbents [24]. Therefore, it is significant to explore novel method to coat magnetic materials, which can guarantee both good separation and adsorption performance.

Graphene oxide (GO) is a two-dimensional (2D) nanomaterial with a large planar size and an atomic thickness. Moreover, GO possesses large specific surface area (SAA) and abundant oxygenated functional groups, which provide an excellent platform to load magnetic nanoparticles and act as ideal adsorption sites for various organic matters and metal ions [25–27]. A multitude of researches have been successfully performed to graft magnetic nanoparticles on GO to adsorb pollutants [28–31]. Furthermore, the abundant carboxyl group of GO can chemically react with the amine group of PLGA, and then form chemical bond between GO and PLGA [32]. However, to the best of our knowledge, the use of β-CD/PLGA functionalized magnetic graphene oxide (MGO) materials for adsorption of pollutants has rarely been reported. Based on the above considerations, therefore, β-CD/PLGA was coated with MGO and its adsorption behavior was explored in this article. The preparation process is schematically exhibited in Scheme 1.

In this work, β-CD/PLGA modified MGO (CGMG) was prepared successfully and characterized by Fourier transform infrared (FT-IR) spectroscopy, X-ray photoelectron spectroscopy (XPS), Raman spectroscopy, X-ray diffraction (XRD), magnetization hysteresis curve, and Brunauer-Emmett-Teller (BET) area. The adsorption behavior of E2 onto CGMG (i.e. the adsorption kinetics, isotherms, and thermodynamics) and the factors (i.e., pH and ionic strength) potentially affecting the adsorption were investigated. Moreover, the regeneration of CGMG was also explored to assess its reusability.

## 2. Experimental section

### 2.1. Materials

E2 (98% purity, molecular structure presented in Fig. S1) was obtained from Sigma-Aldrich Corporation. β-CD, PLGA, p-toluenesulfonyl chloride (PTSC), acetonitrile, ethylenediamine (EDA), N-hydroxysuccinimide (NHS), dimethyl sulfoxide (DMSO), dicyclohexylcarbodiimide (DCC), 4-dimethylaminopyridine, phosphate buffer solution (PBS), 1-ethyl-3-(3-dimethylaminopropyl) carbodiimide hydrochloride (EDC), methanol and acetone were of analytical reagent grade and purchased from Aladdin Industrial Corporation (Shanghai, China). Graphite powder (particle size $\leqslant$ 30 μm), ferric chloride ($FeCl_3$), and ferrous chloride ($FeCl_2$) were supplied by Tianjin Hengxin Chemical Preparation Co., Ltd. (Tianjin, China). All the solutions were prepared by Milli-Q water under ambient conditions.

### 2.2. Preparation of adsorbents

#### 2.2.1. Preparation of $NH_2$-β-CD

(p-Tolylsulfonyl)-β-cyclodextrin (TsO-β-CD) was synthesized by following the literature method [33]. Briefly, β-CD (10.0 g) was suspended in Milli-Q water (150 mL), and sodium hydroxide (NaOH, 4.0 g) in Milli-Q water (7 mL) was instilled dropwise over 6 min. The suspension became homogeneous and slightly yellow before the addition process was complete. PTSC (2.6 g) in acetonitrile (10 mL) was then added slowly over 8 min, which resulted in immediate formation of white precipitate. After 3 h of stirring at room temperature, the precipitate was removed through filtration, and the filtrate was adjusted to neutral pH with HCl. Then, it was kept overnight at 4 °C in a refrigerator. After that, the resulting white precipitate was collected through filtration and rinsed 3 times with acetone. Finally, TsO-β-CD was obtained by drying at 60 °C for 48 h under vacuum. Further, TsO-β-CD (5 g) was dissolved in excess amount of EDA (30 mL) at 75 °C for 4 h to realize nucleophilic reaction. The mixture was cooled down to room temperature, which led to the formation of the $NH_2$-β-CD by reprecipitation of the solution via addition of excessive amount of acetone (30 mL). The precipitate was repeatedly dissolved in a mixture of Milli-Q water (90 mL) and methanol (30 mL), and poured into acetone (30 mL). Finally, the product $NH_2$-β-CD was dried at 50 °C for 3 d in a vacuum oven.

#### 2.2.2. Preparation of β-CD/PLGA

PLGA (0.6 g) and NHS (242 mg) were dissolved in anhydrous DMSO (5 mL), and then DCC (432 mg) and a catalytic amount of 4-dimethylaminopyridine were introduced into the reaction solution. Subsequently, the reaction mixture was vigorously stirred at room temperature for 3 d. Further, the solution of $NH_2$-β-CD (2.3 g) in DMSO was instilled dropwise into the reaction system followed by constant stirring for 5 d. Then the solution was diluted with Milli-Q water (20 mL), and the dicyclohexylurea was filtered off. Besides, the filtrate was further purified by dialysis (with a

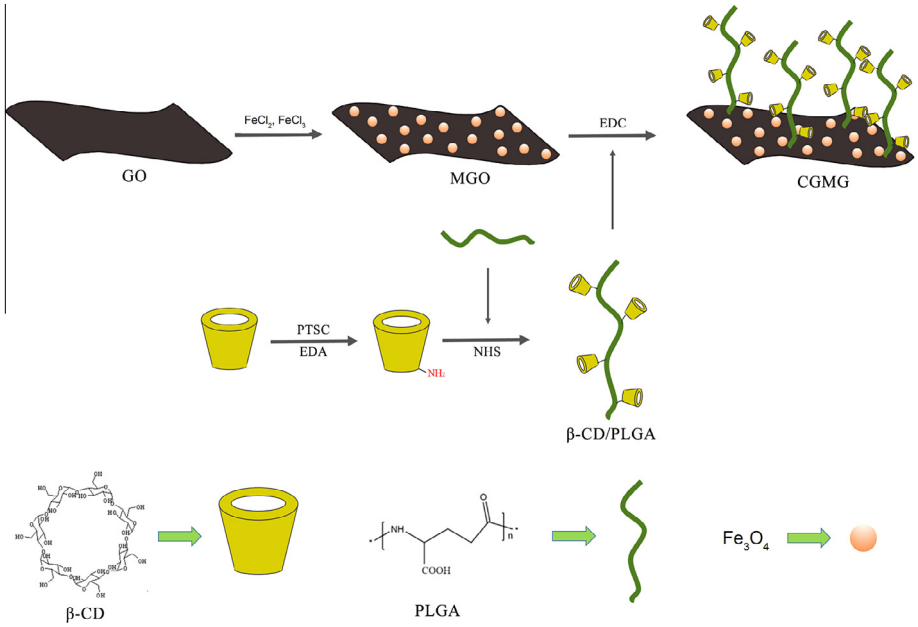


**Scheme 1.** Schematic representation of synthesis processes of the CGMG composite.

molecular weight cutoff of 7000 Da) against deionized water at room temperature for 3 d to remove the residual $NH_2$-β-CD. Finally, the dry product was obtained by vacuum drying the above mentioned solution [20].

### 2.2.3. Preparation of MGO

GO nanosheets were synthesized from natural powder graphite via the modified Hummers method [26,34]. The details about the synthesis of GO nanosheets were provided in the Supplementary material. Further, MGO was prepared using coprecipitation method [35]. Briefly, GO solution (400 mL, 5 mg/mL) was added to mixed solution (200 mL) of $FeCl_3$ (0.1 mol/L) and $FeCl_2$ (0.05 mol/L), and was vigorously stirred by addition of ammonia solution (pH was adjusted to 10) under 85 °C for 45 min. Then chemical precipitation was achieved, and the precipitate was rinsed with Milli-Q water until the solution was almost neutral, which resulted in the formation of MGO suspension.

### 2.2.4. Preparation of β-CD/PLGA/MGO

MGO (0.1 g) was dispersed in PBS (5.0 mL, pH 6), and then continuously stirred and ultrasonicated for 30 min. Afterward, β-CD/PLGA (0.1 g) and EDC (0.03 g) were introduced into the MGO dispersion and the mixed system was sonicated at 4 °C for 1 h. The mixture was stirred continuously for 48 h at room temperature. Finally, the obtained β-CD/PGA/MGO was rinsed several times with Milli-Q water and dried for 48 h under vacuum [32].

## 2.3. Characterization methods

FT-IR spectra were recorded on a spectrophotometer (Nicolet 5700 Spectrometer) with the range from 500 to 4000 $cm^{-1}$ using the KBr pellet technique. XPS was performed using an ESCALAB 250Xi X-ray photoelectron spectrometer (Thermo Fisher, USA) with the scanning range of 0–1000 eV. Raman spectra were obtained by using a Raman spectrometer (Labram-010, FAR) with the scanning range of 300–2000 $cm^{-1}$ at 532 nm excitation wavelength. XRD measurement was carried out using an X-ray diffractometer (Rigaku D/max-2500, Japan) with CuKa radiation (λ = 0.154 nm) at a voltage of 40 kV and a current of 30 mA. The average crystallite size was estimated using the Debye-Scherrer equation (detailed information provided in Supplementary material). The magnetic property was determined with magnetization curve via a vibrating sample magnetometer (Lake Shore 7410, USA). The BET surface area and the pore size distribution were obtained by using $N_2$ adsorption and desorption (Quantachrome, USA) at 77 K over a relative pressure ranging from 0.0955 to 0.993. The surface morphologies of the adsorbents were measured by scanning electron microscopy (SEM) (JSM-7001F, Japan).

## 2.4. Adsorption experiments

All batch sorption experiments were performed in a water bath shaker at a shaking speed of 160 rpm. The E2 stock solution was prepared through dissolving E2 in methanol and the desired E2 working solutions were diluted from E2 stock solutions with Milli-Q water. Moreover, in order to avoid the cosolvent effect, the volume of methanol in the working solutions was maintained at less than 0.1%. For all the adsorption experiments, CGMG (5 mg) was added in E2 solution (100 mL). After being shaken for 12 h in a water bath shaker with a shaking speed of 160 rpm, the mixture was separated by using a permanent magnet. Effect of initial solution pH on E2 adsorption was investigated at initial E2 concentration of 2 mg/L and 298 K. The pH was adjusted to desired values through adding negligible volumes of NaOH or HCl solution. Effect of ionic strength on the adsorption of E2 was examined by adding NaCl to 2 mg/L E2 solutions containing with concentrations ranging from 0.001 to 0.1 M at 298 K and pH 7.0.

The concentrations of E2 were measured through an F-4500 fluorescence spectrophotometer (Hitachi, Japan) as described in the Supplementary material. The amount of E2 adsorbed per unit mass of the adsorbent was evaluated based on the mass balance equation as follows:

$$q_e = \frac{(C_o - C_e)V}{m} \quad (1)$$

where $q_e$ (mg/g) is the adsorbed amount of E2 at equilibrium; $C_o$ and $C_e$ (mg/L) stand for the initial and equilibrium concentrations of E2 in the solution, respectively; $V$ (L) is the volume of the E2 solution, and $m$ (g) is the mass of the adsorbent used.

### 2.5. Recycling

To regenerate CGMG, the residues after adsorption were washed three times with NaOH solution (50 mL, 4 wt.%) at 25 °C. Further, the residues were transferred into pure acetone (50 mL), then the vial was sealed by aluminum foil and agitated at 298 K and 160 rpm for 24 h [36]. After drying, the CGMG adsorption capacity was determined via aforementioned processes, and the relative adsorption capacity was calculated by using $q_{e,n}/q_{e,o}$, where $q_{e,n}$ and $q_{e,o}$ were the adsorption capacity of CGMG in the $n$ cycle and without regeneration, respectively.

## 3. Results and discussion

### 3.1. Characterization of materials

The FT-IR spectra of MGO, β-CD/PLGA, and CGMG are shown in Fig. 1a. For MGO, the peaks at 3402, 1725, 1387, 1220, and 1087 $cm^{-1}$ are assigned to the stretching vibrations of O–H, C=O, O=C–O, C–O–C, and C–O bonds, respectively. The peak at 1624 $cm^{-1}$ resulted from the skeletal vibration of the C=C bond. The strong peak at 560 $cm^{-1}$ corresponded to the stretching vibration of Fe–O in $Fe_3O_4$. Thus, it indicated that MGO was prepared successfully. For β-CD/PLGA, the peak at 1052 $cm^{-1}$ was attributed to the vibration of antisymmetric glycosidic $\nu_a$ (C–O–C) of β-CD. The characteristic absorbance peak at 1446 $cm^{-1}$ was assigned to –NHCO– stretching vibration. Compared to the vibration of –NHCO– in PLGA (Fig. S2), the vibration of -NHCO- was expressed differently with respect to size and position, which indicated possible connection of β-CD and PLGA through –NHCO– bond, and successful synthesis of β-CD/PLGA. For CGMG, the presence of Fe-O in $Fe_3O_4$ (at 560 $cm^{-1}$), the antisymmetric glycosidic $\nu_a$ (C-O-C) vibrations (at 1028 $cm^{-1}$), and the –NHCO– stretching vibration (at 1552 $cm^{-1}$) were also observed, indicating successful synthesis of CGMG.

The surface functional groups and chemical composition of CGMG were analyzed by XPS. For XPS spectra of CGMG (Fig. 1b), it revealed that besides peaks of C1s and O1s, two notable peaks attributed to N1s and Fe2p are also observed, which originate from β-CD/PLGA and $Fe_3O_4$ nanoparticles of MGO. Furthermore, the elemental analysis exhibited a significant increase in O/C atomic ratio of CGMG (0.53) compared to that of MGO (0.31), which demonstrated that β-CD/PLGA might have high relative O/C atomic ratio. From the N1s XPS spectrum of CGMG in Fig. S3, a mainly peaks were observed at 389.9 eV which might be attributed the C-NH-C groups originated from β-CD/PLGA. Therefore, it could conclude that both β-CD/PLGA and MGO were successfully grafted onto CGMG.

In the Fig. 1c of Raman spectra, two prominent peaks at ca. 1345 and 1607 $cm^{-1}$ were assigned to the D band and the G band, respectively. The D band relating to the stretching vibration of $sp^3$ carbon atoms results in defects and disorders. However, the G band is related to the stretching vibration of $sp^2$ carbon atoms in a graphitic 2D hexagonal lattice. As well known, the intensity ratio of D band ($I_D$) and G band ($I_G$) could be used to investigate the extent of disorder [37]. The $I_D/I_G$ of CGMG (1.05) was slightly larger than that of GO (0.88), which demonstrated the introduction of β-CD/PLGA into the $sp^2$ carbon network of MGO. As shown in XRD pattern (Fig. 1d), seven intense diffraction peaks for CGMG ($2\theta$ = 30.23, 35.53, 37.66, 43.42, 53.85, 57.17 and 62.84) corresponded to the facets [(2 2 0), (3 1 1), (2 2 2), (4 0 0), (4 2 2), (5 1 1) and (4 4 0)] of the cubic spinel crystal planes of $Fe_3O_4$ (JCPDS card No. 19-0629) [38], respectively. It also indicated that the $Fe_3O_4$ nanoparticles were successfully grafted on CGMG. Besides, the average crystallite size of $Fe_3O_4$ was determined by Debye-Scherrer analysis of the X-ray diffraction data. According to the Debye-Scherrer equation, the average crystallite size, which was calculated based on the XRD pattern (3 1 1), was approximately 26 nm. This indicated that $Fe_3O_4$ was nanocrystalline [39].

To further examine the magnetic properties of CGMG, magnetization hysteresis curve was obtained by using vibrating sample magnetometry (VSM) at room temperature. For Fig. 1e, it showed that the saturation magnetization (Ms) of the CGMG composite was 0.09043 emu/mg, which indicated that CGMG composite exhibited high magnetism and was enough to realize solid–liquid separation via a permanent magnet. The retentivity (Mr) was 0.00614 emu/mg, which indicated rather little residual magnetization when the additive magnetic field was removed and CGMG composite showed a superparamagnetic behavior. Furthermore, the separation performance of CGMG could be demonstrated by the insets shown in Fig. 1e which illustrated that CGMG could be collected from the host liquid through a permanent magnet. Thus, it suggested that CGMG had excellent magnetic properties and might be recycled conveniently.

To examine the SSA of CGMG, the nitrogen adsorption–desorption isotherms were obtained as shown in Fig. 1f. The CGMG composite exhibited higher SSA of 298.9 $m^2/g$, when compared to that of β-CD/PLGA (105.5 $m^2/g$). The increase in SSA for CGMG confirmed that grafting MGO could promote the special surface area of β-CD/PLGA, thus providing more sites for adsorption. The typical SEM images of the GO and CGMG are exhibited in Fig. S4. From Fig. S4a, GO presented the sheet-like structure with the large thickness, smooth surface, and wrinkled edge. After the modification to form the CGMG composite (Fig. S4b), the CGMG had a much rougher surface which indicated that many small magnetic particles and β-CD/PLGA had been assembled on the surface of GO layers with a high density.

### 3.2. Adsorption kinetics

Kinetic investigation illustrates crucial information about the mechanism of E2 adsorption onto CGMG, which is beneficial to research the adsorption rate of adsorbent and control the residual time of entire adsorption reaction. In this work, Fig. 2a exhibits the time dependence of E2 adsorption on CGMG at different initial concentrations. Clearly, a rapid adsorption of E2 occurred during the first 100 min, followed by a slower adsorption until the adsorption equilibrium was obtained in approximately 480 min. The rapid adsorption rate might be attributed to the absence of internal diffusion resistance and the availability of large number of vacant sites for adsorption at the initial stage [40,41].

In order to further detect the detailed information about the adsorption process of CGMG, two kinetic models were used to analyze the experimental data, including pseudo-first-order and pseudo-second-order model. Detailed information about these models was provided in the Supplementary material. The nonlinear fits of pseudo-first-order and pseudo-second-order sorption kinetics are illustrated in Fig. 2a, respectively. The kinetic parameters simulated from these models are provided in Table 1. Clearly, the value of determination coefficients ($R^2$) in pseudo-second-order model was much higher than that in the pseudo-first-order model. The values of root mean square error (*RMSE*) and chi-square test ($\chi^2$) in pseudo-second-order model were lower than those in pseudo-first-order model. Moreover, a more little discrepancy was observed between the experimental and the calculated adsorption capacity in pseudo-second-order model, compared to that in pseudo-first-order model. Thence, it could concluded that the pseudo-second-order kinetic model fitted the adsorption process better than the pseudo-first-order model, suggesting that the adsorption rate depended on chemisorption (i.e., π-π interaction or hydrogen bonding) [34].

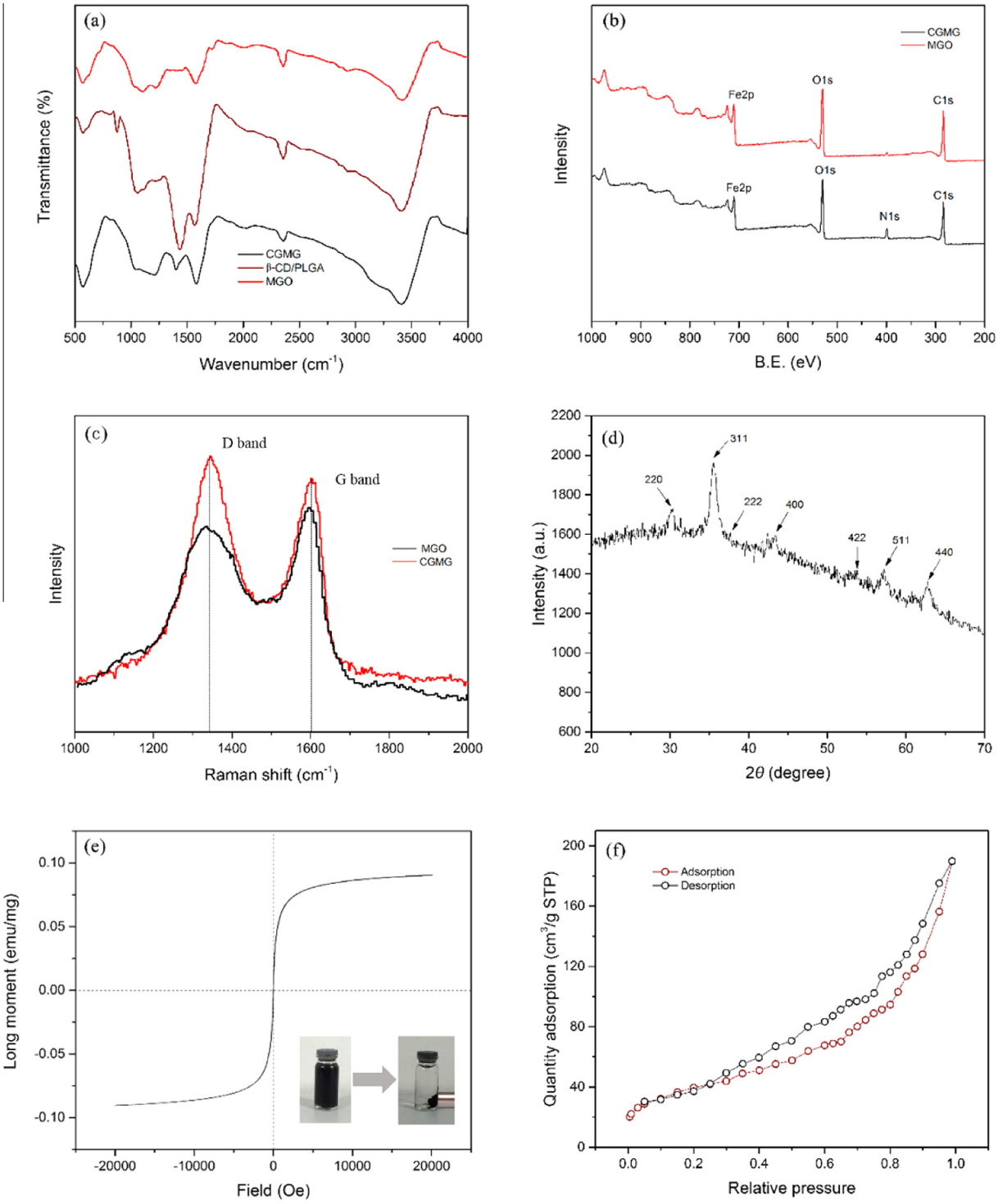


**Fig. 1.** (a) FTIR spectra of MGO, β-CD/PLGA, and CGMG; (b) XPS survey of MGO and CGMG; (c) Raman spectra of GO and CGMG; (d) XRD pattern of CGMG; (e) VSM magnetization curve of CGMG (Insets exhibit the CGMG dispersed in ultrapure water and separated via the external magnetic field); (f) $N_2$ adsorption-desorption isotherms of CGMG.

Since the above kinetic models were not able to identify the mass transfer steps in E2 uptake, intraparticle diffusion model was further examined. Detailed information about this model was provided in the Supplementary material. As illustrated in Fig. 2b, the plots of $q_t$ versus $t^{0.5}$ for the E2 adsorption were multi-linear containing three distinct regions, which suggested multiple steps taking place during the adsorption process. The first section with a sharp curve might be attributed to the transport of E2 from the bulk solution to the external surface of CGMG via film diffusion. The second section exhibited a gradual adsorption stage which was controlled by intraparticle diffusion (from the external surface into the pores of CGMG). The third section was the final equilibrium step where the intraparticle diffusion started to reach saturation [42]. Thus, it could be concluded that both the film

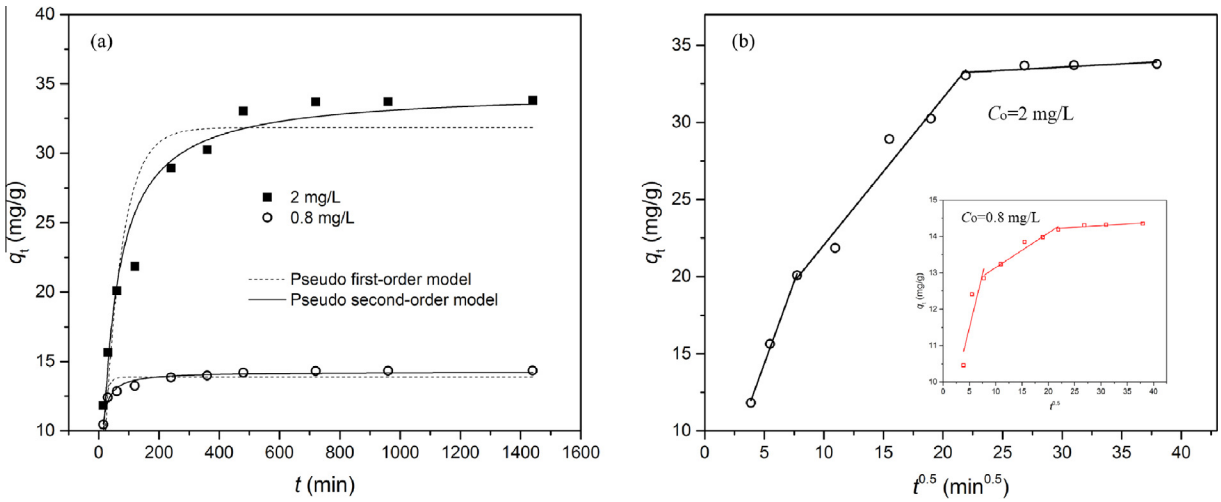


**Fig. 2.** (a) Effect of the contact time on E2 adsorption onto CGMG at different initial concentrations (0.8 and 2 mg/L) and (b) Intraparticle diffusion model for the E2 adsorption onto CGMG ($m/V$ = 0.05 g/L, pH = 7.0, $T$ = 25 °C).

**Table 1**
Kinetic model constants for the E2 uptake by CGMG.

| $C_o$ (mg/L) | Pseudo-first-order | | | | | Pseudo-second-order | | | | |
|---|---|---|---|---|---|---|---|---|---|---|
| | $k_1$ (1/min) | $q_{e,1}$ (mg/g) | *RMSE* | $\chi^2$ | $R^2$ | $k_2$ (g/mg min) | $q_{e,2}$ (mg/g) | *RMSE* | $\chi^2$ | $R^2$ |
| 0.8 | $8.75 \times 10^{-2}$ | 13.87 | 0.54 | 0.29 | 0.81 | $1.30 \times 10^{-2}$ | 14.26 | 0.27 | 0.051 | 0.97 |
| 2 | $1.70 \times 10^{-2}$ | 31.84 | 3.25 | 10.57 | 0.85 | $7.05 \times 10^{-4}$ | 34.50 | 1.83 | 3.34 | 0.95 |

The experimental adsorption capacities at 0.8 and 2 mg/L are 14.35 and 33.80 mg/g, respectively.

diffusion and intraparticle diffusion were involved in the diffusion process, and the intraparticle diffusion was not the sole rate-controlling step in all the stages.

### 3.3. Adsorption isotherms and thermodynamics

In order to better investigate the adsorption mechanisms, the experimental data were further analyzed via two isotherm models, namely, Langmuir and Freundlich models which were described in the Supplementary material. Langmuir model can be used to illustrate homogeneous adsorption, wherein all the adsorption sites have equal adsorbate affinity; however, Freundlich model considers heterogeneous adsorption because of the diversity of the adsorption sites [43]. Fig. 3 shows the adsorption isotherms for the adsorption of E2 onto CGMG at different temperatures, and the relative simulated parameters are listed in Table 2. As can be seen in Table 2, the adsorption experimental data were better fitted by Langmuir model according to the values of $R^2$, *RMSE*, and $\chi^2$. The better simulation of experimental data by Langmuir model demonstrated the monolayer coverage of E2 onto the homogeneous surface of CGMG. Based on the Langmuir model fitting data, the maximum adsorption capacities of CGMG at 298, 313 and 323 K were 85.80, 71.75, and 56.71 mg/g, respectively. The comparisons of maximum adsorption capacities of the CGMG composite obtained in this work with various adsorbents previously studied for the adsorption of E2 were investigated. It illustrated that the E2 adsorption capacity of CGMG at 298 K (85.80 mg/g) was higher than other adsorbents, including single-walled carbon nanotubes (27.5 mg/g) [7], Multi-walled carbon nanotubes (63.15 mg/g) [44] and activated carbon (67.6 mg/g) [4]. The excellent adsorption performance of CGMG could be mainly ascribed to the following factors: (1) there were mass of oxygen-containing functional groups on CGMG (FT-IR and XPS analysis), which might increase the dispersion of CGMG in water and be favorable for generating hydrogen bonding between the hydroxyl of E2 and the oxygen-containing groups on CGMG [34]; (2) the aromatic matrix of GO in CGMG possessing the π-electron acceptor or donor properties could bind hydrophobic portions in E2 through π-π interactions or hydrophobic effect [45].

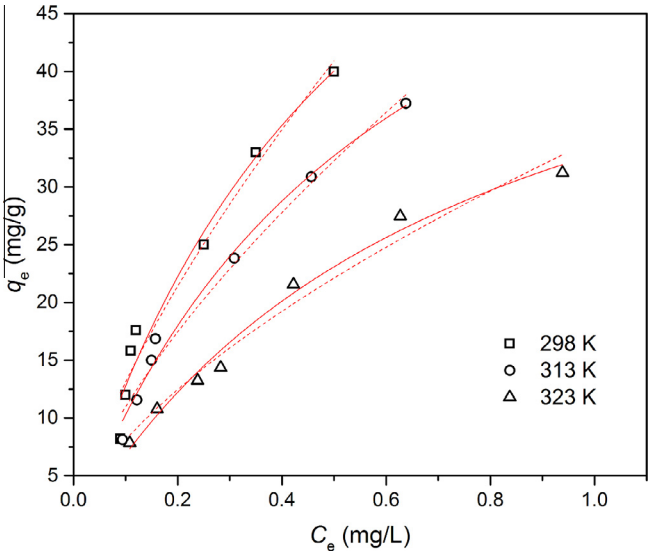


**Fig. 3.** Langmuir and Freundlich non-linear plots of adsorption isotherms for E2 onto the CGMG at 298, 313, and 323 K. The solid lines are Langmuir model simulation, and the dashed lines are Freundlich model simulation ($m/V$ = 0.05 g/L, pH = 7.0, $t$ = 12 h).

Besides, the thermodynamic parameters, such as standard free energy change ($\Delta G°$), standard enthalpy change ($\Delta H°$) and standard entropy change ($\Delta S°$), were calculated from the experimental data via relative equations as described in the Supplementary

**Table 2**
Adsorption isotherm parameters for the E2 uptake by CGMG at 298 K, 313 K and 323 K.

| $T$ (K) | Langmuir model | | | | | Freundlich model | | | | |
|---|---|---|---|---|---|---|---|---|---|---|
| | $q_{max}$(mg/g) | $K_L$ (L/mg) | *RMSE* | $\chi^2$ | $R^2$ | $n$ | $K_F$ ((mg/g)/(mg/L)$^n$) | *RMSE* | $\chi^2$ | $R^2$ |
| 298 | 85.80 | 1.75 | 2.25 | 5.05 | 0.962 | 0.71 | 66.79 | 2.44 | 5.93 | 0.956 |
| 313 | 71.75 | 1.67 | 1.22 | 1.48 | 0.987 | 0.67 | 51.34 | 1.55 | 2.41 | 0.979 |
| 323 | 56.71 | 1.37 | 1.09 | 1.18 | 0.985 | 0.63 | 34.11 | 1.50 | 2.25 | 0.971 |

material. As illustrated in Table S1, the values of $\Delta G°$ were found to be negative at different temperatures, indicating that the adsorption reaction was a spontaneous process [46]. The positive value of $\Delta H°$ proved that the adsorption was exothermic, which was in good agreement with the result shown in Fig. 3 that the adsorption of E2 decreased with the increase in temperature. Besides, the negative $\Delta S°$ value revealed the decreased randomness at solid-liquid interface during the adsorption process [47].

### 3.4. Effect of initial solution pH value

Lewis acid-base interactions (i.e., hydrogen bonding) are frequently sensitive to pH because of the competition between $H^+$ and $OH^-$ ions in aqueous solution [48]. Fig. 4a exhibits that the E2 uptake by CGMG is slightly influenced by pH in the range of 4.2–8.1. Nevertheless, the influence became significant when the pH increased to around 10.1, where the adsorption capacity of E2 reduced to 23.56 mg/g. These phenomena could be associated to the characteristic ionization of E2 molecule in aqueous solution. E2 molecule, as a weak Lewis acid, was strongly dependent upon solution pH during the ionization process. The microspecies distribution of E2 molecule in aqueous solution is illustrated in Fig. 4b. At pH ca. 8.0, E2 molecule started to deprotonate. At pH > 9.2, the deprotonation became evident. The $OH^-$ ion, as strong Lewis base, was capable of easily attracting the proton on the phenolic hydroxyl moiety of E2 molecule and thus led to the deprotonation. Deprotonation would enhance the solubility of E2 in aqueous solution [49,50] and break the hydrogen bonds between E2 and CGMG functional groups via replacement with the protons on E2 molecules. Thus, the ability of E2 molecule to form hydrogen bond with CGMG reduced after deprotonation in aqueous solution. Moreover, CGMG was also negatively charged at high pH levels, resulting in producing repulsive electrostatic interaction between negatively charged E2 anions [34]. The CGMG adsorption process was sensitive to pH, which might limit its applications. Nevertheless, it revealed that exhausted CGMG adsorbent could be conveniently regenerated under specific pH conditions.

### 3.5. Effect of ionic strength

To investigate the influence of ionic strength on the removal of E2 by CGMG, the adsorption capacity was investigated in the presence of sodium chloride. Fig. 5 shows that increasing ionic strength has negligible influence on adsorption of E2 by CGMG. As a general rule, the effect of ionic strength on adsorption resulted in two potential impacts: (1) increasing ionic strength promoted the activity coefficient of hydrophobic organic compounds and reduced their solubility (i.e. salting out effect), which was beneficial to E2 adsorption [51]; (2) the penetration into diffuse double layer surrounding the CGMG surfaces of ions might lead to the elimination of repulsive interaction between the adsorbents and facilitate generation of a more compact aggregation structure (i.e. squeezing-out), which was unfavorable for E2 uptake [34]. Therefore, results might be attributed to the fact that the contribution of salting-out effect to the E2 uptake was equal to that of the squeezing-out effect, or both the salting-out effect and squeezing-out effect were too weak to affect the E2 uptake by CGMG.

### 3.6. Cycles

An ideal adsorbent should have high adsorption ability as well as excellent desorption performance, which reduces the operating cost for the adsorbent application. Thus, the adsorption capacity of the desorbed CGMG was examined by using NaOH and acetone as eluents and re-immersing the regenerated CGMG in E2 solution with known concentration. The adsorption performance of the regenerated CGMG is exhibited in Fig. 6, indicating that the adsorp-

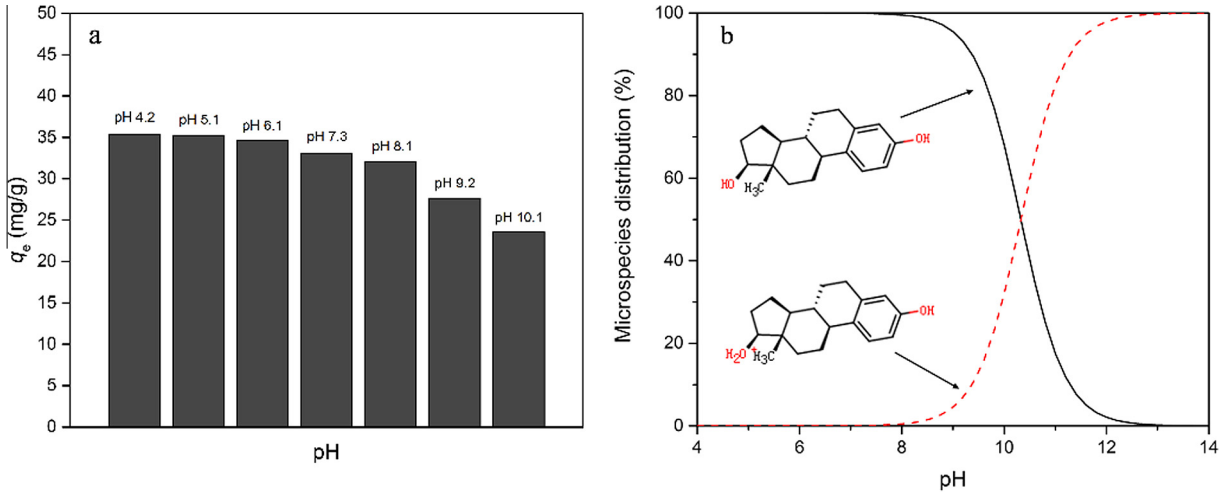


**Fig. 4.** (a) Effect of pH on adsorption E2 by CGMG and (b) distribution of E2 microspecies in aqueous solution as a function of pH ($m/V$ = 0.05 g/L, $C_o$ = 2 mg/L, $t$ = 12 h, $T$ = 25 °C).

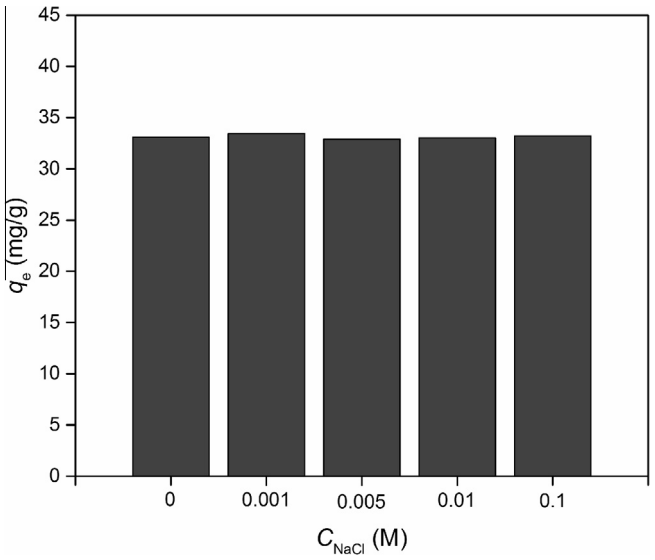


**Fig. 5.** Effect of ionic strength on adsorption E2 by CGMG ($m/V$ = 0.05 g/L, $C_o$ = 2 mg/L, $t$ = 12 h, pH = 7.0, $T$ = 25 °C).

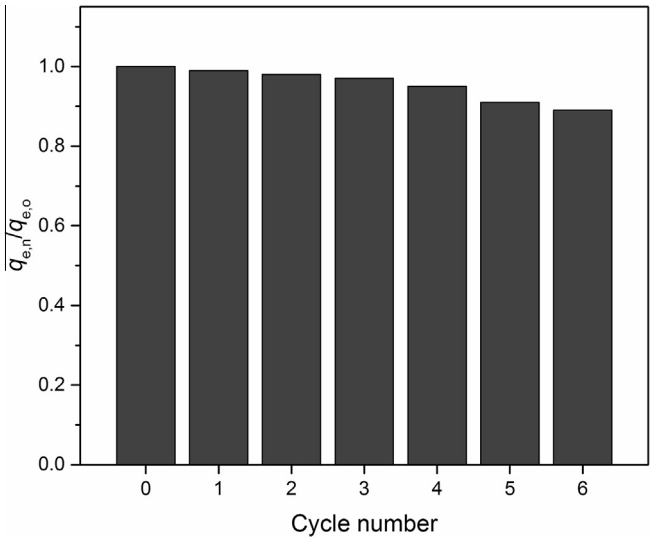


**Fig. 6.** Adsorption ability of E2 by CGMG during six adsorption/desorption cycles ($m/V$ = 0.05 g/L, $C_o$ = 2 mg/L, $T$ = 25 °C).

tion ability of the regenerated CGMG gradually reduces with subsequent uses. The adsorption ability of CGMG reduced only by approximately 11.3% after the 6th cycle, compared to that without regenerated CGMG. This reduction might be ascribed to the loss of binding sites after each desorption procedure. These results demonstrated that the recovery efficiency of CGMG was relatively high with slightly affected by the sixth consecutive regeneration cycles and CGMG could be qualified for practical application.

## 4. Conclusions

In summary, a novel adsorbent, namely, β-cyclodextrin/poly(L-glutamic acid) supported magnetic graphene oxide (CGMG) was fabricated, characterized, and utilized for the removal of 17β-estradiol (E2) from aqueous solution. The magnetization property of CGMG suggested that the adsorbent could be easily separated and collected from reaction solution via an external magnet. The process of adsorption obeyed pseudo-second-order kinetics, and both film diffusion and intraparticle diffusion were involved in the adsorption process. Besides, the equilibrium data were well simulated by the Langmuir model, and the calculated E2 adsorption capacity of CGMG was 85.80 mg/g at 298 K from this model. The E2 adsorption was an exothermic and spontaneous process. Moreover, E2 uptake by CGMG was strongly dependent on pH, and high pH was unfavorable for E2 adsorption. Nevertheless, ionic strength had negligible influence on E2 adsorption. Furthermore, CGMG regeneration experiments indicated its good durability and easy regeneration. Therefore, CGMG is a useful adsorbent for the rapid elimination of E2 from aqueous solution with subsequent uses and could be realized for immediate separation from aqueous solution via external magnetic field.

## Acknowledgements

This work was supported by the Hunan Provincial Innovation Foundation for Postgraduate (Grant No. CX2016B135), the National Natural Science Foundation of China (Grants Nos. 51609268 and 51608208), and the Guangdong Natural Science Foundation (Grants No. 2016A030310246).

## Appendix A. Supplementary data

Supplementary data associated with this article can be found, in the online version, at http://dx.doi.org/10.1016/j.cej.2016.09.067.

## References

[1] Z. Fan, J. Hu, W. An, M. Yang, Detection and occurrence of chlorinated byproducts of bisphenol a, nonylphenol, and estrogens in drinking water of china: comparison to the parent compounds, Environ. Sci. Technol. 47 (2013) 10841–10850.
[2] A.C. Johnson, E. Dumont, R.J. Williams, R. Oldenkamp, I. Cisowska, J.P. Sumpter, Do concentrations of ethinylestradiol, estradiol, and diclofenac in European rivers exceed proposed EU environmental quality standards?, Environ Sci. Technol. 47 (2013) 12297–12304.
[3] H. Tanaka, Y. Yakou, A. Takahashi, T. Higashitani, K. Komori, Comparison between estrogenicities estimated from DNA recombinant yeastassay and from chemical analyses of endocrine disruptors during sewagetreatment, Water Sci. Technol. 43 (2001) 125–132.
[4] T. Fukuhara, S. Iwasaki, M. Kawashima, O. Shinohara, I. Abe, Adsorbability of estrone and 17β-estradiol in water onto activated carbon, Water Res. 40 (2006) 241–248.
[5] Y. Zhang, J.L. Zhou, Removal of estrone and 17β-estradiol from water by adsorption, Water Res. 39 (2005) 3991–4003.
[6] F. Wang, W. Sun, W. Pan, N. Xu, Adsorption of sulfamethoxazole and 17β-estradiol by carbon nanotubes/$CoFe_2O_4$ composites, Chem. Eng. J. 274 (2015) 17–29.
[7] Q. Zaib, I.A. Khan, N.B. Saleh, J.R.V. Flora, Y.G. Park, Y. Yoon, Removal of bisphenol A and 17β-estradiol by single-walled carbon nanotubes in aqueous solution: adsorption and molecular modeling, Water Air Soil Pollut. 223 (2012) 3281–3293.
[8] W. Sun, K. Zhou, Adsorption of 17β-estradiol by multi-walled carbon nanotubes in natural waters with or without aquatic colloids, Chem. Eng. J. 258 (2014) 185–193.
[9] M. Kar, M. Pauline, K. Sharma, G. Kumaraswamy, S. Sen Gupta, Synthesis of poly-L-glutamic acid grafted silica nanoparticles and their assembly into macroporous structures, Langmuir 27 (2011) 12124–12133.
[10] M.P. Melancon, W. Lu, Q. Huang, P. Thapa, D. Zhou, C. Ng, et al., Targeted imaging of tumor-associated M2 macrophages using a macromolecular contrast agent PG-Gd-NIR813, Biomaterials 31 (2010) 6567–6573.
[11] S. Yan, T. Wang, L. Feng, J. Zhu, K. Zhang, X. Chen, et al., Injectable in situ self-cross-linking hydrogels based on poly (L-glutamic acid) and alginate for cartilage tissue engineering, Biomacromolecules 15 (2014) 4495–4508.
[12] J. Ding, C. He, C. Xiao, J. Chen, X. Zhuang, X. Chen, PH-responsive drug delivery systems based on clickable poly (L-glutamic acid)-grafted comb copolymers, Macromol. Res. 20 (2012) 292–301.
[13] D. Bhattacharyya, J.A. Hestekin, P. Brushaber, L. Cullen, L.G. Bachas, S.K. Sikdar, Novel poly-glutamic acid functionalized microfiltration membranes for sorption of heavy metals at high capacity, J. Memb. Sci. 141 (1998) 121–135.
[14] L.H. Reyerson, W.S. Hnojewyj, The adsorption of dry ammonia gas by poly-L-glutamic acid, J. Phys. Chem. 67 (1963) 1945–1948.
[15] H. Wang, Y. Liu, Z. Deng, S. Han, Preparation of $Fe_3O_4$/poly (L-glutamic acid) microspheres and their adsorption of Cu (II) ions, J. Appl. Polym. Sci. (2016).

[16] B. Bhattarai, M. Muruganandham, R.P.S. Suri, Development of high efficiency silica coated β-cyclodextrin polymeric adsorbent for the removal of emerging contaminants of concern from water, J. Hazard. Mater. 273 (2014) 146–154.
[17] L. Fan, C. Luo, M. Sun, H. Qiu, X. Li, Synthesis of magnetic β-cyclodextrin–chitosan/graphene oxide as nanoadsorbent and its application in dye adsorption and removal, Colloids Surf. B Biointerfaces 103 (2013) 601–607.
[18] A.Z.M. Badruddoza, A.S.H. Tay, P.Y. Tan, K. Hidajat, M.S. Uddin, Carboxymethyl-β-cyclodextrin conjugated magnetic nanoparticles as nano-adsorbents for removal of copper ions: synthesis and adsorption studies, J. Hazard. Mater. 185 (2011) 1177–1186.
[19] Y. Tao, J. Dai, Y. Kong, Y. Sha, Temperature-sensitive electrochemical recognition of tryptophan enantiomers based on β-cyclodextrin self-assembled on poly (ι-glutamic acid), Anal. Chem. 86 (2014) 2633–2639.
[20] F. Du, H. Meng, K. Xu, Y. Xu, P. Luo, Y. Luo, et al., CPT loaded nanoparticles based on beta-cyclodextrin-grafted poly (ethylene glycol)/poly (ι-glutamic acid) diblock copolymer and their inclusion complexes with CPT, Colloids Surf. B Biointerfaces 113 (2014) 230–236.
[21] X. Hu, J. Wang, Y. Liu, X. Li, G. Zeng, Z. Bao, et al., Adsorption of chromium (VI) by ethylenediamine-modified cross-linked magnetic chitosan resin: isotherms, kinetics and thermodynamics, J. Hazard. Mater. 185 (2011) 306–314.
[22] Z. Fu, C. He, H. Li, C. Yan, L. Chen, J. Huang, et al., A novel hydrophilic–hydrophobic magnetic interpenetrating polymer networks (IPNs) and its adsorption towards salicylic acid from aqueous solution, Chem. Eng. J. 279 (2015) 250–257.
[23] A. Kara, E. Demirbel, N. Tekin, B. Osman, N. Beşirli, Magnetic vinylphenyl boronic acid microparticles for Cr (VI) adsorption: kinetic, isotherm and thermodynamic studies, J. Hazard. Mater. 286 (2015) 612–623.
[24] J. Li, S. Zhang, C. Chen, G. Zhao, X. Yang, J. Li, et al., Removal of Cu (II) and fulvic acid by graphene oxide nanosheets decorated with $Fe_3O_4$ nanoparticles, ACS Appl. Mater. Interfaces 4 (2012) 4991–5000.
[25] Z. Jin, X. Wang, Y. Sun, Y. Ai, X. Wang, Adsorption of 4-n-nonylphenol and bisphenol-A on magnetic reduced graphene oxides: a combined experimental and theoretical studies, Environ. Sci. Technol. 49 (2015) 9168–9175.
[26] H. Wang, Y. Liu, G. Zeng, X. Hu, X. Hu, T. Li, et al., Grafting of β-cyclodextrin to magnetic graphene oxide via ethylenediamine and application for Cr(VI) removal, Carbohydr. Polym. 113 (2014) 166–173.
[27] H. Yan, H. Wu, K. Li, Y. Wang, X. Tao, H. Yang, et al., Influence of the surface structure of graphene oxide on the adsorption of aromatic organic compounds from water, ACS Appl. Mater. Interfaces 7 (2015) 6690–6697.
[28] N.U. Yamaguchi, R. Bergamasco, S. Hamoudi, Magnetic $MnFe_2O_4$–graphene hybrid composite for efficient removal of glyphosate from water, Chem. Eng. J. 295 (2016) 391–402.
[29] E. Roy, S. Patra, R. Madhuri, P.K. Sharma, Europium doped magnetic graphene oxide-MWCNT nanohybrid for estimation and removal of arsenate and arsenite from real water samples, Chem. Eng. J. 299 (2016) 244–254.
[30] K.Y.A. Lin, W.D. Lee, Self-assembled magnetic graphene supported ZIF-67 as a recoverable and efficient adsorbent for benzotriazole, Chem. Eng. J. 284 (2016) 1017–1027.
[31] L. Cui, Y. Wang, L. Gao, L. Hu, L. Yan, Q. Wei, et al., EDTA functionalized magnetic graphene oxide for removal of Pb (II), Hg (II) and Cu (II) in water treatment: adsorption mechanism and separation property, Chem. Eng. J. 281 (2015) 1–10.
[32] J. Liu, G. Liu, W. Liu, Preparation of water-soluble β-cyclodextrin/poly (acrylic acid)/graphene oxide nanocomposites as new adsorbents to remove cationic dyes from aqueous solutions, Chem. Eng. J. 257 (2014) 299–308.
[33] Z. Yuan, Y. Ye, F. Gao, H. Yuan, M. Lan, K. Lou, et al., Chitosan-graft-β-cyclodextrin nanoparticles as a carrier for controlled drug release, Int. J. Pharm. 446 (2013) 191–198.
[34] L. Jiang, Y. Liu, G. Zeng, F. Xiao, X. Hu, X. Hu, et al., Removal of 17β-estradiol by few-layered graphene oxide nanosheets from aqueous solutions: External influence and adsorption mechanism, Chem. Eng. J. 284 (2016) 93–102.
[35] X. Hu, Y. Liu, G. Zeng, H. Wang, X. Hu, A. Chen, et al., Effect of aniline on cadmium adsorption by sulfanilic acid-grafted magnetic graphene oxide sheets, J. Colloid Interface Sci. 426 (2014) 213–220.
[36] J. Han, W. Qiu, J. Hu, W. Gao, Chemisorption of estrone in nylon microfiltration membranes: adsorption mechanism and potential use for estrone removal from water, Water Res. 46 (2012) 873–881.
[37] D. Dinda, S.K. Saha, Sulfuric acid doped poly diaminopyridine/graphene composite to remove high concentration of toxic Cr (VI), J. Hazard. Mater. 291 (2015) 93–101.
[38] J. Kim, S. Oh, S.Y. Kwak, Magnetically separable magnetite–lithium manganese oxide nanocomposites as reusable lithium adsorbents in aqueous lithium resources, Chem. Eng. J. 281 (2015) 541–548.
[39] X. Sun, C. Zheng, F. Zhang, Y. Yang, G. Wu, A. Yu, et al., Size-controlled synthesis of magnetite ($Fe_3O_4$) nanoparticles coated with glucose and gluconic acid from a single Fe (III) precursor by a sucrose bifunctional hydrothermal method, J. Phys. Chem. C 113 (2009) 16002–16008.
[40] X. Hu, Y. Liu, H. Wang, G. Zeng, X. Hu, Y. Guo, et al., Adsorption of copper by magnetic graphene oxide-supported β-cyclodextrin: effects of pH, ionic strength, background electrolytes, and citric acid, Chem. Eng. Res. Des. 93 (2015) 675–683.
[41] G.K. Ramesha, A.V. Kumara, H.B. Muralidhara, S. Sampath, Graphene and graphene oxide as effective adsorbents toward anionic and cationic dyes, J. Colloid Interface Sci. 361 (2011) 270–277.
[42] Z. Wu, H. Zhong, X. Yuan, H. Wang, L. Wang, X. Chen, et al., Adsorptive removal of methylene blue by rhamnolipid-functionalized graphene oxide from wastewater, Water Res. 67 (2014) 330–344.
[43] H. Lee, D. Kim, J. Kim, M.K. Ji, Y.S. Han, Y.T. Park, et al., As (III) and As (V) removal from the aqueous phase via adsorption onto acid mine drainage sludge (AMDS) alginate beads and goethite alginate beads, J. Hazard. Mater. 292 (2015) 146–154.
[44] W. Sun, C. Zhang, N. Xu, J. Ni, Effect of inorganic nanoparticles on 17β-estradiol and 17α-ethynylestradiol adsorption by multi-walled carbon nanotubes, Environ. Pollut. 205 (2015) 111–120.
[45] F. Pendolino, E. Parisini, S. Lo Russo, Time-dependent structure and solubilization kinetics of graphene oxide in methanol and water dispersions, J. Phys. Chem. C 118 (2014) 28162–28169.
[46] L. Ai, C. Zhang, Z. Chen, Removal of methylene blue from aqueous solution by a solvothermal-synthesized graphene/magnetite composite, J. Hazard. Mater. 192 (2011) 1515–1524.
[47] M. Alkan, M. Doğan, Y. Turhan, Ö. Demirbaş, P. Turan, Adsorption kinetics and mechanism of maxilon blue 5G dye on sepiolite from aqueous solutions, Chem. Eng. J. 139 (2008) 213–223.
[48] J. Han, W. Qiu, Z. Cao, J. Hu, W. Gao, Adsorption of ethinylestradiol (EE2) on polyamide 612: molecular modeling and effects of water chemistry, Water Res. 47 (2013) 2273–2284.
[49] M. Clara, B. Strenn, E. Saracevic, N. Kreuzinger, Adsorption of bisphenol-A, 17β-estradiole and 17α-ethinylestradiole to sewage sludge, Chemosphere 56 (2004) 843–851.
[50] J. Virkutyte, R.S. Varma, V. Jegatheesan, Treatment of Micropollutants in Water and Wastewater, IWA Publishing, 2010, ISBN 10:1843393166.
[51] S. Zhang, T. Shao, S.S.K. Bekaroglu, T. Karanfil, Adsorption of synthetic organic chemicals by carbon nanotubes: effects of background solution chemistry, Water Res. 44 (2010) 2067–2074.